Optics Letters

Large-angle two-dimensional grating with hybrid mechanisms

Junyu Zou,[1] Ziqian He,[1] Qian Yang,[1] Kun Yin,[1] Kun Li,[2] and Shin-Tson Wu[1,*]

[1]College of Optics and Photonics, University of Central Florida, Orlando, Florida 32816, USA
[2]GoerTek Electronics, 5451 Great America Parkway, Suite 301, Santa Clara, California 95054, USA
*Corresponding author: swu@creol.ucf.edu

Received 11 December 2020; revised 15 January 2021; accepted 26 January 2021; posted 27 January 2021 (Doc. ID 417468); published 12 February 2021

We demonstrate a large-diffraction-angle two-dimensional (2D) grating based on cholesteric liquid crystal (CLC). One dimension is a polarization volume grating (PVG) working in the Bragg regime, which is produced by a patterned photoalignment layer. The other dimension is a CLC grating working in the Raman–Nath regime, which is introduced by CLC self-assembly under a weak anchoring energy condition. The condition for the coexistence of the CLC Raman–Nath grating (RNG) and PVG is analyzed, and the efficiency and grating period of the CLC RNG are also characterized. Potential application of this 2D grating for enlarging the eyebox of augmented reality displays is discussed.

https://doi.org/10.1364/OL.417468

Cholesteric liquid crystal (CLC) exhibits a periodic structure along the helical axis due to its intrinsic self-assembly property. The pitch length P is the distance when the liquid crystal (LC) directors rotate 360° along the helical axis. When a CLC layer is well aligned in a homogeneous cell, its helical axis will be perpendicular to the substrate, as Fig. 1(a) shows, and Bragg condition can be established for the circularly polarized light with the same handedness [1,2]. Since all the LC directors are uniform in the planes parallel to the substrate, such a CLC is called planar state, and it works as a circular polarization selective reflector [3]. If the CLC is grating patterned, then the Bragg plane will be tilted, and the polarization selective reflector will become a polarization selective deflector. This idea has been proven with photoalignment in 2016 [4]. Based on this principle, a large-deflection-angle polarization volume grating (PVG) is also proposed and fabricated [5,6]. Further study has shown that when the CLC is grating patterned, not only the Bragg plane is tilted but also the helical axis is slanted [7] as Fig. 1(b) depicts. Because of its large deflection angle, PVG has attracted lots of attention in waveguide-based augmented reality systems [8–10].

On the other hand, CLC Raman–Nath grating (RNG) has aroused great research interest since late 1990s [11–25]. A fascinating feature of this grating is that it is formed by CLC self-organization, which is a kind of CLC fingerprint texture [11,12]. This kind of grating was first found in a homogenously aligned CLC cell [13,14]. Periodic stripes with a period of Λ can be obtained in the presence of an appropriate electric field, as a transition state between the planar state and the homeotropic state. In [13], this CLC RNG is also called the in-plane modulated state (M state). In [14], the CLC RNG in a homogenous cell is considered to have a lying helix structure, as Fig. 2(a) shows. However, if the CLC RNG is fabricated in a semi-free film or hybrid cell, the helical axis is still perpendicular to the substrate at the bottom layer. It is the self-adopted periodic distortion near the top surface, which leads to the formation of the CLC RNG [18,19] shown in Fig. 2(b). For the semi-free film, the air-LC interface also acts as aligning layer to promote vertical alignment. The CLC RNG direction can be influenced by the alignment direction [13], electric field [20,21], light field [15,18,22], temperature [20], and CLC pitch length and thickness [20]. On the other hand, the CLC RNG period depends on the electric field [14], light field [23], temperature [24], and CLC pitch length and thickness [25].

The formation of the CLC RNG benefits from the intrinsic property of CLC, and these periodic stripes can be introduced under a proper electric field, optical irradiation, or hybrid alignment. All these factors are external stimuli, which impair the anchoring energy of planar state CLC. In the PVG fabrication process, the grating patterned photoalignment leads to a tilted Bragg plane and helical axis, which is also a method to impair the planar anchoring energy. Therefore, we expect that CLC RNG can be formed in PVG.

In this Letter, we experimentally demonstrate the coexistence of the CLC RNG and PVG, which results in a reflection-type two-dimensional (2D) grating. The 2D grating is fabricated

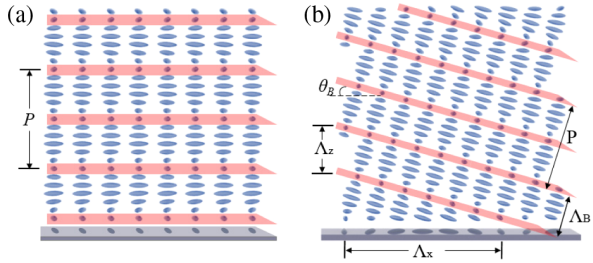

Fig. 1. Schematic of (a) the planar state CLC and (b) the reflective PVG. P is the pitch length, Λ_x is the period of grating pattern in photoalignment layer, Λ_B is the Bragg period, θ_B is the tilted angle of Bragg plane, and Λ_z is the vertical period.

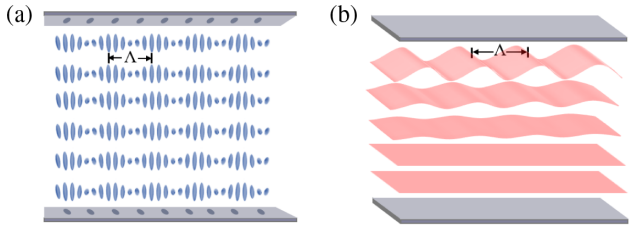

Fig. 2. Schematic of the CLC RNG structure in (a) a homogeneous cell with a weak electric field and (b) a hybrid cell.

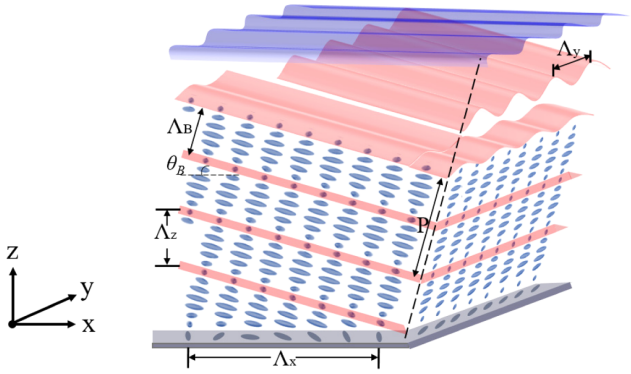

Fig. 3. Schematic of the proposed 2D grating structure, where Λ_y is the CLC RNG period, and other parameters have been defined in Fig. 1. The bottom layer is a PVG, and the top layer is a CLC RNG. Because the LC molecular orientation in the CLC RNG is complicated, we use the cholesteric plane (pink surface) to represent its structure. The blue color on the top indicates the film surface. All the pitch and pitch length appearing later in this paper mean the P in this figure.

based on a polymerized semi-free mesogenic film. Each dimension shows a different grating mechanism. The bottom layer is a photoalignment PVG, and the top layer is a self-adopted CLC RNG, as Fig. 3 depicts. The direction of the PVG is the same as the photoalignment grating pattern (x direction), while the CLC RNG (y direction) is perpendicular to the PVG.

The fabrication process of our proposed 2D grating is the same as that of the PVG [6,7]. First, we spin-coated 0.2 wt. % brilliant yellow (dissolved in dimethyl-formamide) on a cleaned glass substrate, which works as the photoalignment material. Then, the substrate was grating patterned in the optical setup shown in Fig. 4. Thereafter, a reactive mesogen mixture (RMM) was spin-coated on the alignment layer. The solute of this RMM consists of reactive mesogen (RM257 from LC Matter, 93.8–94.6 wt. %), chiral dopant (S5011 from HCCH, 1.9–2.7 wt. %), and photo-initiator (Irgacure 651 from BASF, 3.5 wt. %). Different pitch lengths can be obtained by adjusting the chiral dopant concentration, so that the central wavelengths can appear at the desired RGB bands. In the RMM mixture, the solute was dissolved in toluene, and the ratio of solute to solvent varied from 1:2 to 1:8 in order to achieve different film thicknesses. Next, the spin-coated RMM sample substrate was cured by a UV light under nitrogen environment to attain a stabilized polymer film. More fabrication details can be found in [7].

Figure 5(a) shows the surface patterns of a 2D grating through a polarized optical microscope (Nikon L150). The grating structure is clearly observed. The dark and bright stripes along the y direction are formed by the PVG, whose grating period Λ_x

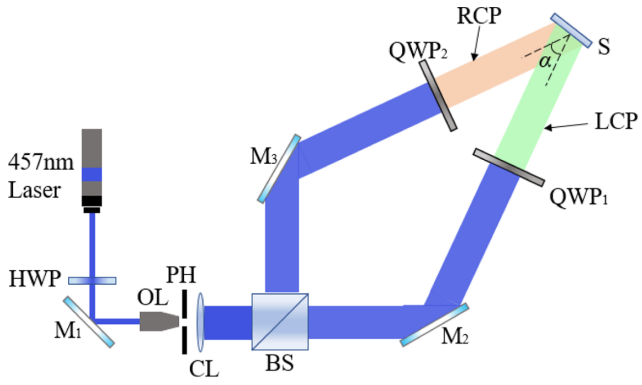

Fig. 4. Experimental setup for fabricating the proposed 2D grating patterns using photoalignment. HWP, half-wave plate; OL, objective lens; CL, collimating lens; QWP, quarter-wave plate; R/LCP, right/left handed circular polarized light; M, dielectric mirror; PH, pinhole; BS, beam splitter; S, sample substrate.

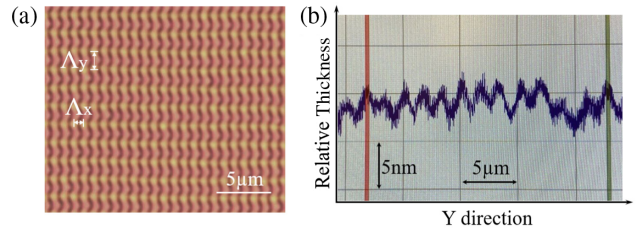

Fig. 5. Surface patterns of the fabricated 2D grating: (a) observed grating structure from a polarized optical microscope and (b) measured surface profile along the y direction by a profilometer. This grating was fabricated at $\alpha = 30°$ with 1.9% chiral dopant, and its cholesteric pitch is 0.405 μm.

is around 0.9 μm. The value of Λ_x is determined by the angle α shown in Fig. 4, and we set $\alpha = 30°$ when the PVG alignment pattern was exposed. The valleys (red parts) and hills (yellow parts) in the image represent the structure of CLC RNG, whose grating period Λ_y is around 1.6 μm. Furthermore, we also used a profilometer (Bruker DektakXT) to measure the surface profile of the sample along the y direction, and results are shown in Fig. 5(b). From the measured profile, the wave-like period is obvious, and the average period is around 1.6 μm, which is consistent with the result measured through the microscope. It is worth mentioning that the periodic surface relief in Fig. 5(b) does not imply the CLC RNG is a surface grating. It is the existence of the CLC RNG near the top surface of the film that results in this surface relief with the same period.

The optical setup for characterizing the fabricated 2D grating is illustrated in Fig. 6(a). A $\lambda = 635$ nm linearly polarized laser beam is normally incident on the sample at point O with an incident power of about 600 μW. That means the left-handed circular polarization (LCP) component is about 300 μW. Upon diffraction, three spots (A, B, and C) are observed on the screen. In Fig. 6(a), laser pointer L, incident point O, and diffraction point A are in the horizontal ($x - z$) plane while the connection line of diffraction points B and C is perpendicular to the $x - z$ plane. Point A is the diffraction from the PVG, whose working principle follows the Bragg volume grating shown in Fig. 6(b). In the figure, θ_B is the tilted angle of Bragg plane, which is determined by the grating pattern period Λ_x and Bragg period Λ_B as

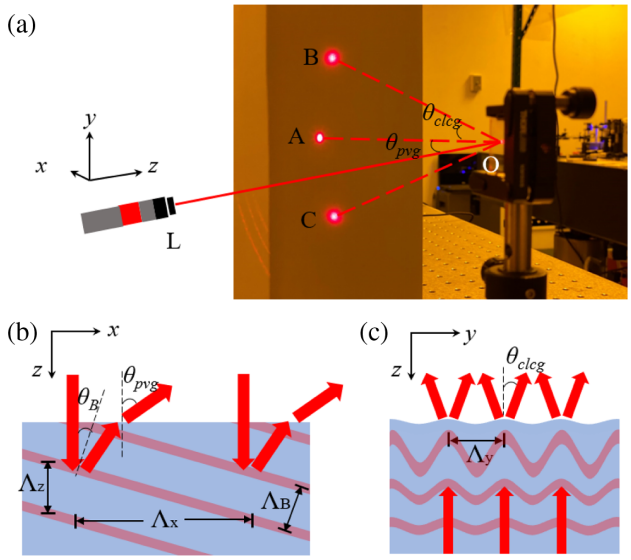

Fig. 6. (a) Diffraction performance of a fabricated 2D grating with a laser ($\lambda = 635$ nm) at normal incidence, where θ_{pvg} is the diffraction angle of the PVG and θ_{clcg} is the diffraction angle of the CLC RNG. The schematic of the working principle for (b) the PVG and (c) the CLC RNG. All the parameters have been defined before.

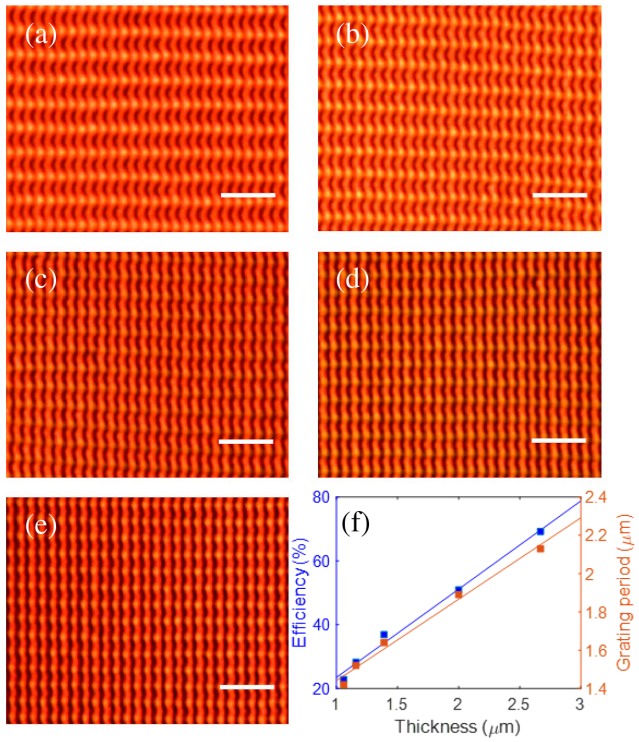

Fig. 7. Polarized optical microscope image on the surface of a fabricated 2D grating with different CLC RNG periods: (a) 2.13 μm, (b) 1.89 μm, (c) 1.64 μm, (d) 1.52 μm, and (e) 1.42 μm. The scale bar is 5 μm. (f) Measured efficiency and grating period of the CLC RNG as the film thickness increases. All these gratings were fabricated at $\alpha = 30°$ with 1.9% chiral dopant, and their cholesteric pitch is 0.405 μm.

$\theta_B = \sin^{-1}(\Lambda_B/\Lambda_X)$. The diffraction angle can be calculated by grating equation $\theta_{pvg} = \sin^{-1}(\lambda/\Lambda_X)$, and the calculated result is $\theta_{pvg} = 44.9°$. It matches well with the measured diffraction angle, around 45°. Points B and C are the ±1 diffraction orders of the CLC RNG, and they are symmetrical along point A. Figure 6(c) depicts the working principles of a CLC RNG. According to the grating equation, the calculated diffraction angle is 23.4°, which agrees well with our measured data (23°). Moreover, the polarization states of all three diffractive beams are perfectly circular [Stokes parameter $S_3 = -1$ (LCP), measured by a polarimeter PAX1000VIS from Thorlabs]. Our measured optical power at A, B, and C points are 116 μW, 35 μW, and 33 μW, respectively. The total diffraction efficiency for the ±1 orders of the CLC RNG is 37%. From Fig. 6(c), the surface periodic ridge structure can hardly contribute to the diffraction efficiency of CLC RNG because the amplitude is too small (5 nm). According to finite-difference time-domain (FDTD) method, the efficiency of this surface relief grating is much lower than 0.1%. Therefore, the diffraction should originate from the periodic undulation of cholesteric planes [pink band in Fig. 6(c)], which in turn leads to the refractive index modulation.

In fact, the periodicity and efficiency of the CLC RNG are related to the film thickness. Figures 7(a)–7(e) show the images of 2D gratings with thickness varying from ∼2.7 μm to 1 μm, and the period of the CLC RNG changes from 2.13 μm to 1.42 μm. All these 2D gratings have a PVG grating period of 0.9 μm, which is determined solely by the exposure setup (once the exposure wavelength $\lambda = 457$ nm and angle α in Fig. 4 are fixed, the period of the PVG grating period will not change). Figure 7(f) depicts the trend of CLC RNG period and efficiency with film thickness. As the film thickness increases, both the CLC RNG period and efficiency increase approximately linearly.

However, the existence of the CLC RNG needs to meet certain conditions. If the film is too thin, then the anchoring energy is too strong to form the CLC RNG, leaving only the PVG [Fig. 8(a)]. On the other hand, if the film is too thick, the CLC RNG cannot align well [Fig. 8(b)]. Moreover, the existence condition of the CLC RNG is also related to the pitch length. According to previous observation in LC cells, the d/p ratio should be controlled within a certain range so that the CLC RNG can be formed [13,20,25], which means the optimal thickness and the pitch length have a linear relation. To obtain more specific conditions, we independently change the film thickness and pitch length to see how seriously these two parameters influence the existence condition of the CLC RNG, respectively. In the experiment, we set the angle α in Fig. 4 at 35° ($\Lambda_x = 0.76$ μm) and fabricated samples with different pitch lengths and thicknesses. The samples that form the CLC RNG are plotted in Fig. 8(c) (experimental data). The corresponding central wavelength of the pitch length changes from 0.46 μm to 0.64 μm, which covers most of the visible spectrum. The average thickness of these samples at a certain pitch length is considered as the optimal thickness at the corresponding pitch length. According to the fitting, the optimal thickness and the pitch length satisfy the quadratic function: $d_{opt} = 242p^2 - 134p + 19.16$ (both d_{opt} and p are in μm). This indicates that the existence conditions of the CLC RNG are different in the LC cell and the polymer film. In our case, the existence condition of this CLC RNG is more sensitive to p. The pink band in Fig. 8(c) is the region that the CLC RNG can be formed. The upper and lower limits of this region also fit well with different quadratic equations. In addition, the color

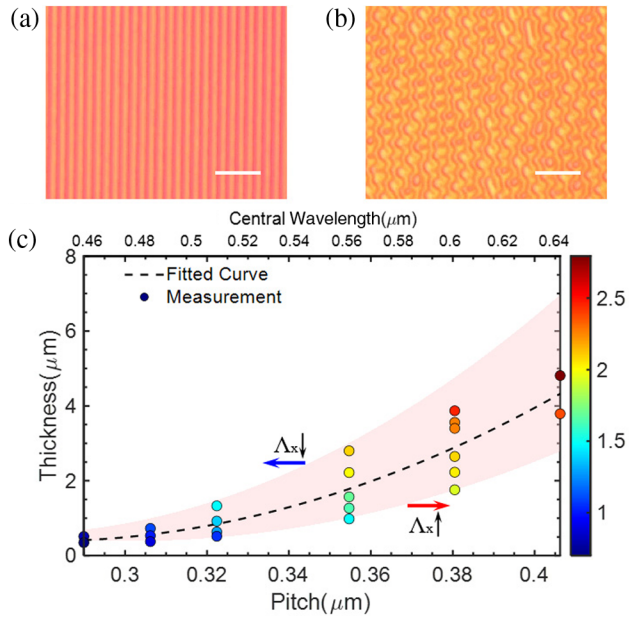

Fig. 8. Polarized optical microscope image on the surface of fabricated grating when the thickness is (a) too thin or (b) too thick to form the 2D grating. The scale bar is 5 μm. (c) Measured data and fitting results for analyzing the existence conditions of the proposed 2D grating. The color bar indicates the grating period of the CLC RNG.

bar at the righthand side of Fig. 8(c) indicates the CLC RNG grating period. From Fig. 8(c), we also find that the larger the pitch length, the larger the CLC RNG grating period, when the thickness is fixed.

Since this is a 2D grating, the existence condition of the CLC RNG is also influenced by the PVG period (Λ_x). During device fabrication, we notice that as the PVG period (Λ_x) increases, the CLC RNG formation region [pink band in Fig. 8(c)] will shift toward right (i.e., redshift). Conversely, if the PVG period decreases, the CLC RNG formation region will blueshift. Specifically, if the angle α in Fig. 4 is 30° ($\Lambda_x = 0.9$ μm), then the pink band will shift toward the right, which will lead the CLC RNG's optimal thickness for red and green pitch lengths to a convenient range for spin-coating (0.5 μm to 3 μm), but it is too thin for the blue band. If the angle α in Fig. 4 is 40° ($\Lambda_x = 0.66$ μm), the pink band will move to the left. This will make the CLC RNG forming thickness for green and blue pitch lengths fabricable, but the red band is beyond the range by spin-coating. In [6,7], the angle α is larger than 60° so that the blueshift in the pink band of Fig. 8(c) is noticeable. Moreover, the film is too thin to form the CLC RNG when the pitch length is in the visible spectral region. This explains why these authors did not see the CLC RNG in their works.

Since this 2D grating increases the number of diffracted beams, it can be a potential candidate for enlarging the eyebox of an augmented reality display [26]. Because each dimension is based on a different mechanism, the grating period of the PVG is determined by the photoalignment pattern, while the grating period and efficiency of the CLC RNG can be slightly tuned by the film thickness and the pitch length. Therefore, the position and the intensity of diffracted beams can be optimized for different applications.

In conclusion, we have experimentally demonstrated that a self-adopted CLC RNG can be formed within the photoalignment PVG, so that a reflective 2D grating with a large diffraction angle can be obtained. The grating periods from submicron to 2.8 μm are achieved for the CLC RNG with different pitch lengths and thicknesses. The diffraction angle of this grating can be calculated by the grating equation, and the experimental results agree with calculation very well. Since this CLC RNG is PVG-based, the diffracted beams are ideally circularly polarized. The existence conditions of this kind of grating are also investigated. The relation between optimal thickness and pitch length fits well with a quadratic function, which is different from previous observation in the LC cell. Potential application of such a 2D grating for near-eye displays is foreseeable.

Funding. Goertek Electronics.

Disclosures. The authors declare no conflicts of interest.

REFERENCES

1. D. W. Berreman and T. J. Scheffer, Phys. Rev. Lett. **25**, 577 (1970).
2. W. S. John, W. J. Fritz, Z. J. Lu, and D. K. Yang, Phys. Rev. E **51**, 1191 (1995).
3. D. J. Broer and J. Lub, "Cholesteric polarizer and manufacture thereof," U.S. patent 5,506,704 (9 April 1996).
4. J. Kobashi, H. Yoshida, and M. Ozaki, Nat. Photonics **10**, 389 (2016).
5. Y. Weng, D. Xu, Y. Zhang, X. Li, and S. T. Wu, Opt. Express **24**, 17746 (2016).
6. Y. H. Lee, K. Yin, and S. T. Wu, Opt. Express **25**, 27008 (2017).
7. Y. H. Lee, Z. He, and S. T. Wu, J. Opt. Soc. Am. B **36**, D9 (2019).
8. Y. Weng, Y. Zhang, J. Cui, A. Liu, Z. Shen, X. Li, and B. Wang, Opt. Lett. **43**, 5773 (2018).
9. Y. H. Lee, T. Zhan, and S. T. Wu, Virtual Reality Intell. Hardware **1**, 10 (2019).
10. J. Xiong, K. Yin, K. Li, and S. T. Wu, Adv. Photon. Res. **2**, 2000049 (2021).
11. S. W. Kang, S. Sprunt, and L. C. Chien, Appl. Phys. Lett. **76**, 3516 (2000).
12. H. K. Bisoyi, T. J. Bunning, and Q. Li, Adv. Mater. **30**, 1706512 (2018).
13. D. Subacius, P. J. Bos, and O. Lavrentovich, Appl. Phys. Lett. **71**, 1350 (1997).
14. D. Subacius, S. V. Shiyanovskii, P. J. Bos, and O. D. Lavrentovich, Appl. Phys. Lett. **71**, 3323 (1997).
15. Z. G. Zheng, Y. Li, H. K. Bisoyi, L. Wang, T. J. Bunning, and Q. Li, Nature **531**, 352 (2016).
16. R. Eelkema, M. M. Pollard, N. Katsonis, J. Vicario, D. J. Broer, and B. L. Feringa, J. Am. Chem. Soc. **128**, 14397 (2006).
17. A. Ryabchun, D. Yakovlev, A. Bobrovsky, and N. Katsonis, ACS Appl. Mater. Interfaces **11**, 10895 (2019).
18. L. L. Ma, W. Duan, M. J. Tang, L. J. Chen, X. Liang, Y. Q. Lu, and W. Hu, Polymers **9**, 295 (2017).
19. A. Ryabchun and A. Bobrovsky, Adv. Opt. Mater. **6**, 1800335 (2018).
20. C. H. Lin, R. H. Chiang, S. H. Liu, C. T. Kuo, and C. Y. Huang, Opt. Express **20**, 26837 (2012).
21. H. C. Jau, T. H. Lin, Y. Y. Chen, C. W. Chen, J. H. Liu, and A. Y. G. Fuh, Appl. Phys. Lett. **100**, 131909 (2012).
22. A. Ryabchun, A. Bobrovsky, J. Stumpe, and V. Shibaev, Adv. Opt. Mater. **3**, 1273 (2015).
23. H. C. Jau, Y. Li, C. C. Li, C. W. Chen, C. T. Wang, H. K. Bisoyi, T. H. Lin, T. J. Bunning, and Q. Li, Adv. Opt. Mater. **3**, 166 (2015).
24. L. Zhang, L. Wang, U. S. Hiremath, H. K. Bisoyi, G. G. Nair, C. V. Yelamaggad, A. M. Urbas, T. J. Bunning, and Q. Li, Adv. Mater. **29**, 1700676 (2017).
25. S. N. Lee, L. C. Chien, and S. Sprunt, Appl. Phys. Lett. **72**, 885 (1998).
26. T. Lin, T. Zhan, J. Zou, F. Fan, and S. T. Wu, Opt. Express **28**, 38616 (2020).